Glucosamine to gold nanoparticles binding studied using Raman spectroscopy

Vlasta Mohaček-Grošev [*,a], *Sandro Brljafa* [b], *Marko Škrabić* [c], *Ivan Marić* [d], *Vesna Blažek Bregović* [e], *Vincenzo Amendola* [f], *Polona Ropret* [g] *and Anita Kvaček Blažević* [h]

[a] Center of Excellence for Advanced Materials and Sensing Devices, Research Unit New Functional Materials, Ruđer Bošković Institute, Bijenička cesta 54, 10000 Zagreb, Croatia, e-mail: Vlasta.Mohacek.Grosev@irb.hr

[b] Osnovna škola Antuna Gustava Matoša, Albrechtova bb, 10000 Zagreb, Croatia, e-mail: sandro.brljafa@gmail.com

[c] Department of Physics and Biophysics, School of Medicine, University of Zagreb, Šalata 3b, 10000 Zagreb, Croatia, e-mail: marko.skrabic@mef.hr

[d] Radiation Chemistry and Dosimetry Laboratory, Ruđer Bošković Institute, Bijenička cesta 54, 10000 Zagreb, Croatia, e-mail: imaric@irb.hr

[e] Laboratory for Optics and Optical Thin Films, Division of Materials Physics, Ruđer Bošković Institute, Bijenička cesta 54, 10000 Zagreb, Croatia, e-mail: vblazek@irb.hr

[f] Department of Chemical Sciences, University of Padova, Padova I -35131, Italy, e-mail: vincenzo.amendola@unipd.it

[g] Institute for the Protection of Cultural Heritage of Slovenia, Research Institute, Poljanska cesta 40, 1000 Ljubljana, Slovenia, e-mail: polona.ropret@zvkds.si

[h] Faculty of Electrical Engineering, Computer Science and Information Technology Osijek, Kneza Trpimira 2b, 31000 Osijek, Croatia, e-mail: akvacek@ferit.hr

Abstract

The binding of glucosamine in water solutions of glucosamine hydrochloride mixed with clean colloidal gold nanoparticles obtained by laser ablation in liquid was studied using surface-enhanced Raman scattering (SERS), dynamic light scattering (DLS) and UV-VIS spectroscopy.

The average size of dried gold nanoparticles was (20 ± 4) nm determined by averaging the sizes observed in transmission electron microscopy micrographs, which is smaller than the average size of gold nanoparticles in water solution as determined by DLS: (52 ± 2) nm. Upon adding the glucosamine solutions to gold colloid, average hydrodynamic diameter of ions was slightly larger for 0.1 mM glucosamine solution (55 ± 2 nm), while it increased to (105 ± 22) nm in the case of 1 mM solution, and was (398 ± 54) nm when 10 mM glucosamine solution was added.

Most prominent Raman bands observed both for 0.1 mM and 1 mM glucosamine solutions were located at 1165 cm^{-1}, 1532 and 1586 cm^{-1} and assigned to C-N coupled with C-C stretching, and C-NH_3^+ deformation angles bending. In SERS spectrum of 1 mM $GlcN^+$ solution, two strong bands at 999 and 1075 cm^{-1} were found and attributed to C-O_{ring} stretching coupled with C-NH_3^+ bending (999 cm^{-1}) and to dominantly C-O stretching vibration. The differences in SERS spectra are attributed to different number of glucosamine molecules that attach to gold nanoparticles and their orientation with respect to the metal particle surface, partly due to presence of beta anomers protonated at anomeric oxygen position. The assignment of glucosamine bands was further corroborated by comparison with vibrational spectra of alpha and beta glucose and of polycrystalline powder of glucosamine hydrochloride. For all three substances comprehensive calculation of vibrational density of states was conducted using density functional theory. Benchmark bands for polycrystalline glucose anomers distinction are 846 and 915 cm^{-1} for alpha glucose, and 902 cm^{-1} for beta glucose. However, the bands observed in SERS spectra of 0.1 mM glucosamine solution at 831, 899, and 946 cm^{-1} or in 1 mM solution at 934 cm^{-1} cannot be easily identified as belonging either to alpha or beta glucosamine anomer, due to complexity of atomic motions involved.

keywords: glucosamine, clean AuNPs, SERS, density functional theory, DLS, UV-VIS

manuscript prepared for submission to Spectrochimica Acta A: Molecular and Biomolecular Spectroscopy

Introduction

Being among smallest aminosugars, glucosamine is often found in biopolymers such as chondroitin, chitosan or hyaluronic acid. Nowdays, people use it as a nutritional supplement for appeasing arthritical pain in joints, with disputed effectiveness [1]. It is a direct precursor in the formation of glycosaminoglycans in cartilage [2], and can also serve as an inhibitor of glycoprotein biosynthesis of influenza virus [3]. Hyaluronic acid is a constituent of corpus vitreus [4], is present in renal modulla [5], and contributes to mediation of solute diffusion through the extracellular space [6]. Recently, polymers most suitable for enhancing the wound healing have been investigated [7-10]. In particular, chitosan which is a copolymer of glucosamine and N-acetyl glucosamine units, is found to be among most prominent polymers with biodegradability, biocompatibility, non-toxicity and antimicrobial properties [10].

Together with thiols and phosphines, amines display affinity for gold surfaces [11]. This property has been used in applying ultraviolet light on glucosamine-functionalized gold nanoparticles for reducing microbial activity [12], and for achieving an increased contrast in computed tomography images when glucosamine coated gold nanoparticles were injected [13]. Amine functionalized gold nanoparticles were used by Shikha et al. to bind carboxylic groups of aspartic or glutamic acids present in the lipase enzyme [14]. Liu and Hsing used glucosamine functionalized gold nanoparticles for specfic targeting of cancer cells [15].

Having in mind these latest applications of glucosamine attached to gold nanoparticles (AuNPs), we have undertaken a study of glucosamine ($GlcN^+$) to AuNPs binding by performing surface-enhanced Raman spectroscopy (SERS), dynamic light scattering (DLS), zeta potential measurements and UV-VIS spectroscopy. Transmission electron microscopy was used for bare AuNPs average size determination, while the hydrodynamic size of gold ions in water and glucosamine solutions was determined by dynamic light scattering. To ensure that no other chemical substances interfere with the interaction between $GlcN^+$ and the surface of the nanoparticles, we used AuNPs obtained by laser ablation in liquid (LAL). In this way, the AuNPs are produced from the laser ablation of pure gold plate in a 10^{-4} M NaCl solution in bidistilled water [16,17], without the need for stabilizing agents or other adsorbed molecules deriving from the degradation of wet-chemistry synthesis precursors. The laser generated AuNPs possess a negative zeta potential [18], hence zeta potential measurements were undertaken to verify the binding of glucosamine to gold by observing progressive reduction of negative charge of gold nanoparticles with the increase of glucosamine concentration.

Normal modes of glucosamine were studied by performing *ab initio* calculation for neutral form of the free glucosamine $GlcN^o$, and density functional calculation for the crystal of glucosamine hydrochloride in which glucosamine occurs in the form of charged $GlcN^+$ ion. The same form of ions is present in water solutions of glucosamine at pH 4.5 [19]. These calculations were compared with observed Raman and infrared spectra of polycrystalline glucosamine hydrochloride and 1M water solution of glucosamine, which enabled a confident assignment of observed bands and provided a

basis for interpretation of surface-enhanced Raman spectra of glucosamine on gold nanoparticles. SERS spectra of 1 mM and 0.1 mM glucosamine water solutions mixed with gold colloid provided several well distinguished bands suitable for further research on glucosamine sensing.

Experimental

Gold colloids

The AuNPs were obtained by laser ablation synthesis in liquid using 1064 nm laser pulses (6ns, 50 Hz) of a Q-switched laser, focused with a f= 150 mm lens to a fluence of 5 J/cm^2 on a 99.99 % pure Au plate dipped in a 10^{-4} M NaCl solution in bidistilled water [16,17].

Gold colloids were prepared for transmission electron microscopy (TEM) by separating supernatant from the sediment using UNIVERSAL 320 centrifuge with relative centrifugal force (RFC) of 720g during 30 minutes. Supernatant was applied to hexagonal copper grids and left to dry for several hours before TEM examination using a JEOL JEM 1011 microscope. The applied voltage was 80 kV with magnifications up to 300 000 times. ImageJ software was used for determination of the average dimension of particles [20].

Preparation of water solutions of glucosamine hydrochloride ($GlcN^+ \cdot Cl^-$)

Glucosamine hydrochloride in the form of polycrystalline powder, with purity better than 99 %, was purchased from Sigma and used without further purification. Stock solution of 1M concentration was prepared by weighing 0.2156 g of powder and mixing it with 1 mL of extra pure water demineralized by SG Reinstwasser System RO 6 Sp to conductivity of 0.055 μS/cm. From this solution, 10 mM, 2 mM, 1 mM and 0.1 mM glucosamine solutions were obtained by proportional dilution.

pH value of the stock solution was determined to be 4.5 using Edge Blue pH meter from Hanna instruments.

UV-VIS spectroscopy of glucosamine and gold colloid solutions

For absorption in the UV-VIS region, three samples were prepared as follows: 200 μL from each of the sample (pure AuNPs, 2 mM and 10 mM solution of $GlcN^+$) were diluted with 2 mL of extra pure water in quartz cuvette and placed in the scattering chamber of Perkin Elmer Lambda 25 UV-VIS spectrometer operating in the range 190 – 1100 nm. Spectra were recorded in the 190 – 900 nm interval. All glucosamine solutions with pH equal to 4.5 were colourless.

Dynamic light scattering (DLS) and zeta potential measurements

The average hydrodynamic diameters of AuNPs, pure and in 1:1 v/v water mixtures, and of $GlcN^+$-AuNP particles were measured using Zetasizer Ultra instrument manufactured by Malvern Panalytical, equipped with a 632.8 nm He-Ne laser, using the Multi-Angle Dynamic light Scattering (MADLS) technology. MADLS performs analysis at three different scattering angles (174.7°, 90.0° and 12.78°) and compiles the data into a single integrated measurement. The measurements were performed in DTS0012 standard 10 mm plastic cells. Hydrodynamic diameters were calculated on the basis of intensity distributions, and the results are presented as mean values of 3 measurements. Zeta potential measurements were performed using electrophoretic light scattering in DTS1080 folded capillary cells. The values of zeta potentials are given as a mean value of three measurements.

Raman spectroscopy of pure substances

In order to validate bands, Raman spectra of polycrystalline glucosamine HCl were obtained under the microscopes of two different instruments. The first was a Horiba JobinYvon T64000 operating in triple subtractive configuration with 1800 grooves per mm for each grating and with 532 nm laser excitation, with 50x LWD objective. The second was LABRAM HR800 with two gratings, 600 and 1800 grooves/mm with 785 nm laser excitation and 100x objective. The observed Raman bands are listed in Supplementary Table S1. Spectrum of the 1M glucosamine water solution was acquired by collecting the inelastically scattered light in the 90° geometry from the sample tube positioned in the macro chamber of the T64000 spectrometer. Raman spectra of polycrystalline α-D- and β-D-glucose were obtained using micro chamber of the T64000 instrument, just like for glucosamine HCl powder.

Surface-enhanced Raman spectroscopy (SERS)

Samples for SERS were prepared by diluting 1 M stock solution of $GlcN^+ \cdot Cl^-$ to 0.1 mM, 1 mM and 10 mM concentrations. 5 µl of each was mixed with 5 µl of sediment of centrifuged gold colloid and placed on a silicon substrate under the microscope. Spectra of droplets were recorded with Renishaw INVIA instrument using 785 nm laser excitation with a 10 seconds accumulation time, by averaging 5 acquisitions.

Infrared spectroscopy

Polycrystalline powders of α-D- and β-D-glucose and of glucosamine · HCl were each mixed with KBr in a mortar in approximately 1:100 ratio and pressed into pellets. Infrared spectra in transmission mode and 400 – 4000 cm^{-1} interval were collected using Perkin Elmer Spectrum GX with a 1 cm^{-1} resolution and repetition rate of 40 scans.

Computational details

The structure of free glucosamine molecule $C_6H_{11}O_5NH_2$, ($GlcN^0$), was optimised and its normal modes calculated using Gaussian09 program suite [21] with B3LYP functional and 6-31++G(d,p) basis set. The crystal structure of $C_6H_{14}NO_5^+ \cdot Cl^-$ ($GlcN^+ \cdot Cl^-$) as redetermined by Harrison et al [22] served as a starting point for optimizing atomic positions within the unit cell of $P2_1$ space group with a = 7.1474 Å, b = 9.2140 Å, c = 7.7650 Å, β = 112.884° and Z =2, using CRYSTAL09 program [23,24]. Electron correlation was implemented as by Perdew, Burke and Ernzerhof [25], (code name PBE) while exchange part of the density functional was that of Perdew et al [26] (code name PBESOL). Factor of mixing of the old trial wavefunction with the new one (FMIXING) was set to 30 %. The basis set for nitrogen, carbon, oxygen and hydrogen atoms was taken from the work of Gatti et al. on urea [27], and the basis set for chlorine was from the work of Apra et al. on NaCl [28]. The output of the frequency calculation for glucosamine hydrochloride crystal is part of the Supplementary Information. One can upload it and open with the web application CRYSPLOT [29] in order to view the atomic motions in each of the normal modes.

The same procedure was applied in determination of phonon density of states for α-D- and β-D-glucose. Both glucose anomers crystallize in $P2_12_12_1$ space group with four molecules per unit cell, but with different cell parameters [30,31].

Results

In Fig.1A particle size ditribution obtained from transmission electron microscopy micrographs (Fig.1B) is presented. The average diameter is calculated as (20 ± 4) nm using program ImageJ [20].

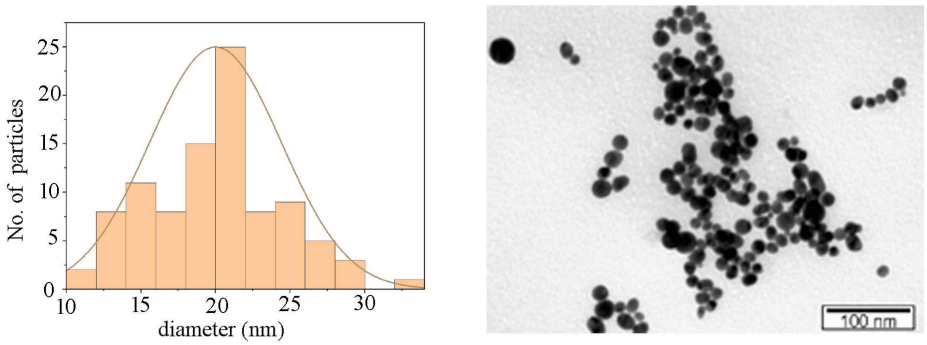

(A) (B)

Figure 1. (A) Histogram showing the distribution of particle sizes obtained with ImageJ software. Total number of particles was 95. (B) TEM micrograph of gold nanoparticles obtained by LAL synthesis in 10^{-4} M NaCl aqueous solution.

The value of average particle hydrodynamic diameter as calculated from DLS measurements of gold colloid is (52 ± 2) nm. The stability of gold colloid particles was assessed also after 1:1 dilution with ultrapure water by measuring again the average diameter with DLS, which resulted only in a very small increment to $\bar{d}$ = (57 ± 5) nm. No significant difference was found in the values of zeta potential of pure gold colloid and 1:1 water diluted one; zeta potential of pure gold colloid was (-31.2 ± 2.3) mV, while on dilution with water it was (-32.0 ± 2.6) mV. Upon adding glucosamine solution, the average particle diameter as determined by DLS was (55 ± 2 nm) for 0.1 mM solution, it increased to (105 ± 22) nm in the case of 1 mM solution, and was (398 ± 54) nm when 10 mM glucosamine solution was mixed with gold colloid. Thicker glucosamine layers with increasing glucosamine concentrations resulted in reduction of zeta potential, which from negative value of (-31.2 ± 2.3) mV for pure gold colloid shifted to (-29.5 ± 1.4) mV in the case of 0.1 mM glucosamine solution, became (-14.7 ± 0.6) mV for 1 mM solution and was practically neutral (-1.8 ± 1.0) mV when most concentrated glucosamine solution was added (10 mM solution). On visual inspection, when 10 mM $GlcN^+$ solution is mixed with AuNPs, it becomes greyish-blue and loses its red colour. Another indication that binding of glucosamine to gold is taking place is obtained from the UV-VIS spectra of glucosamine solutions mixed with gold colloid (Fig.2A).

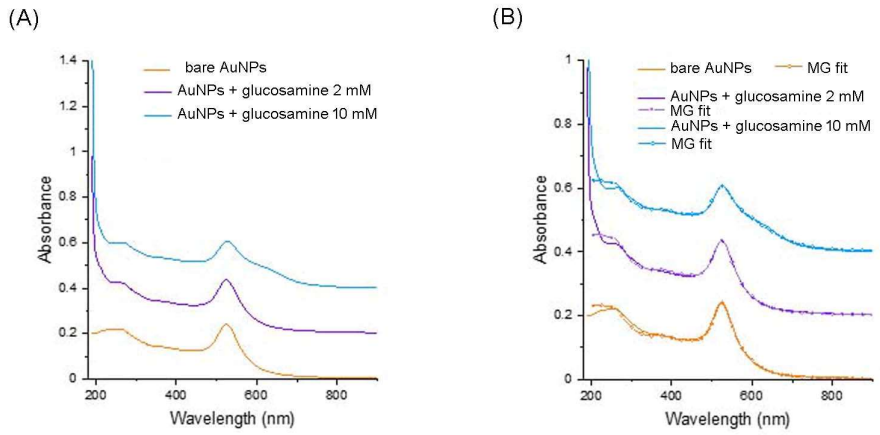

Figure 2. (A) Comparison of UV-VIS spectra of pure gold colloid (yellow) with spectrum of 2 mM glucosamine/colloid mixture (violet) and 10 mM glucosamine/colloid mixture (blue). A shoulder on 625 nm is visible in the spectrum of 10 mM $GlcN^+$-AuNP solution. Spectra were vertically shifted for clarity. (B) Mie-Gans fitting (open circles) of the three spectra suggesting that the fraction of nonspherical nanoparticles is similar in the bare AuNP and 2 mM glucosamine colloid mixture (27 – 21 %), while it increases in the 10 mM glucosamine/colloid mixture (62 %) due to aggregation.

It is worth noticing that the spectrum of bare AuNPs only shows the surface plasmon band typical of spherical gold nanoparticles, centered at 522 nm, and the shoulder due

to gold interband transitions at shorter wavelengths, without any other absorption in the UV region that is typically associated to the presence of organic stabilizers or synthesis byproducts [32]. Instead, when the 2 mM glucosamine solution is added to the AuNPs, an absorption egde appears at 190 – 200 nm, ascribable to the optical absorption of the compound. The absorbance of this edge proportionally increases in the 10 mM glucosamine solution UV-VIS spectrum. Spectroscopically, the original maximum at 522 nm observed for pure gold colloid is shifted to 524 nm in the case of 2 mM $GlcN^+$ solution, and 526 nm for 10 mM $GlcN^+$-AuNP solution, in addition to the appearance of a shoulder at 625 nm that is indicative of nanoparticle aggregation [33].

This is further substantiated by the fitting of the experimental spectra with a code based on the Mie theory for spherical nanoparticles and the Gans model for non-spherical particles [33] (Fig.2B), which confirmed the increase of the fraction of nonspherical particles (i.e. aggregates) in the 10 mM AuNP-$GlcN^+$ mixture (62 %) compared to the 2 mM AuNP-$GlcN^+$ mixture and the bare AuNP (27-21 %).

Two representative SERS spectra of glucosamine-AuNP are displayed in Fig.3, for 0.1 mM and 1 mM concentrations. A strong band in both spectra at 520.7 cm^{-1} corresponds to TO optical phonon of the silicon crystal substrate onto which droplets were placed before spectra were recorded. Spectra consist of broad overlapping bands with some strong bands in common: the 1165 cm^{-1}, 1532 cm^{-1} and 1580 cm^{-1} bands. In SERS spectrum of 1 mM solution there is a strong band at 1075 cm^{-1} which is absent or very weak in the spectrum of 0.1 mM solution. In order to gain insight into the nature of these modes, we performed a normal mode calculation for the free glucosamine molecule ($GlcN^0$) which disposes with $–NH_2$ group, as well as phonon calculation for the glucosamine hydrochloride crystal in which glucosamine has $–NH_3^+$ form ($GlcN^+$).

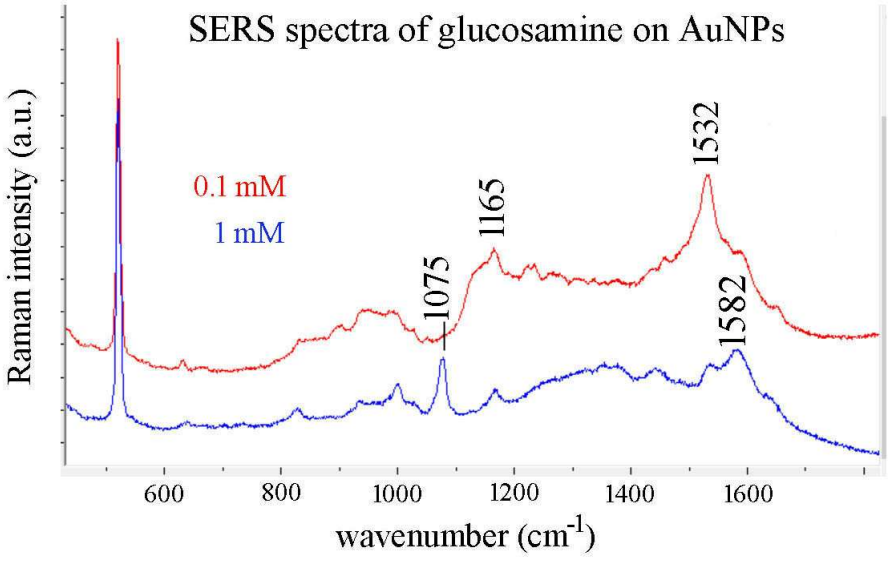

Figure 3. Surface-enhanced Raman spectra of glucosamine 0.1 mM and 1 mM solutions with gold colloid. Spectra are normalized to the same intensity of silicon at 520.7 cm^{-1}. Laser excitation 785 nm.

Glucosamine also takes the same charged form in the 1 M water solution at pH 4.5 [34], which was the reason for undertaking the calculation of the solid state glucosamine hydrochloride phonons. Raman spectra of the 1M water solution of glucosamine and the polycrystalline powder are compared in Fig.4, while the infrared spectrum of polycrystalline glucosamine is shown in Supplementary Fig.S1. All of the observed bands are compared with the calculated ones in the Supplementary Table S1. In view of the strong bands observed in SERS spectra at 1532 and 1582 cm^{-1} (Fig.3), we can compare Raman and infrared spectra of polycrystalline alpha and beta glucose with that of $GlcN^{+}\cdot Cl^{-}$, in the interval 1500 – 1650 cm^{-1}. Only in the glucosamine spectrum there are three rather weak bands, and they are assigned to C-NH_3^{+} angle deformation modes (Fig.5, Fig.S1). In SERS spectrum of the 0.1 mM solution there are bands at 1532, 1563, 1586 and 1652 cm^{-1}, all much stronger compared to corresponding bands of the crystal. The band observed at 1075 cm^{-1} in the spectrum of 1 mM solution is assigned to C-O stretching and glucose ring C-C stretching motion, while the C-N stretching and C-C stretching motions dominate the normal mode assigned to the 1165 cm^{-1} band.

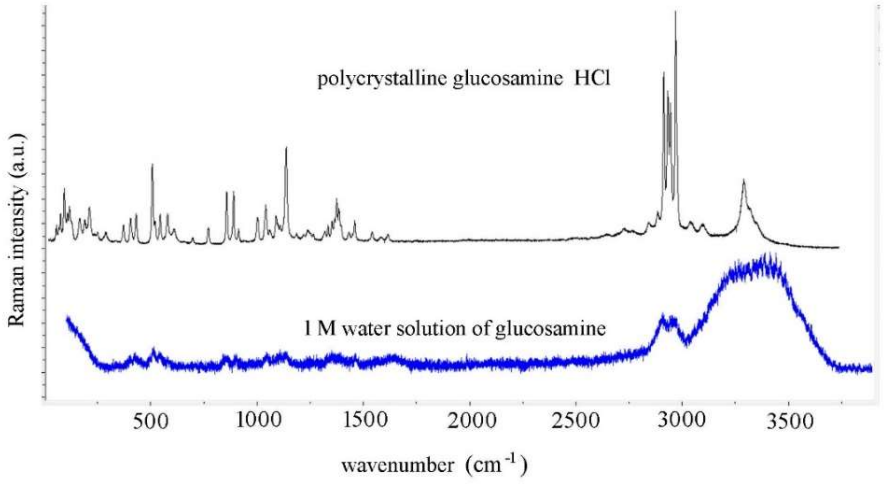

Figure 4. Comparison of Raman spectra of polycrystalline glucosamine HCl and 1 M water solution of glucosamine. Laser excitation 532 nm.

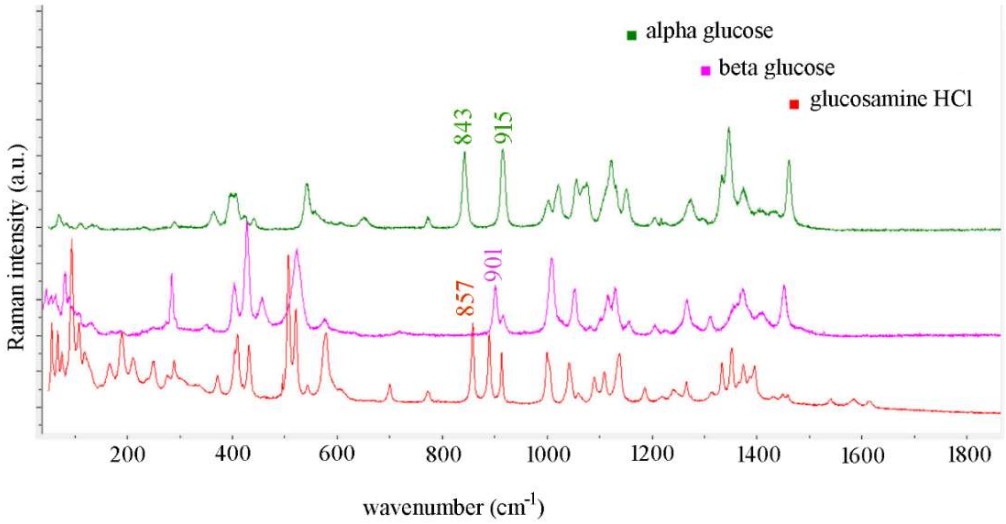

Figure 5. Identification of C-NH_3^+ bending modes in glucosamine in the 1500 – 1650 cm^{-1} interval is possible by comparing spectrum with those of glucose, where these bands, as well as this group, are absent. Laser excitation 532 nm.

Discussion

Glucosamine is an important aminosugar, which displays mutarotation just like glucose: the major anomer of the protonated form $GlcN^+$ is α anomer [34]. Positively charged amino group binds to a negatively charged surface of the gold nanoparticle when gold colloid is mixed with glucosamine water solution, as our results obtained with dynamic light scattering confirm. SERS spectra with resolved bands were obtained from two $GlcN^+$·AuNP solutions: 0.1 mM and 1mM. For 10 mM solution, only unresolved very broad bands appeared, and for concentrations lower than 0.1 mM, no SERS signal was obtained. The orientation of glucosamine molecule with respect to the surface of the gold particle can be estimated on the basis of which normal modes have enhanced intensity. Symmetric motions are often more intense than in ordinary Raman spectrum [35]. In Table 1 the assignment of the observed bands in SERS spectra of 0.1 mM and 1 mM solutions of glucosamine is given, based on phonon calculations for glucosamine hydrochloride crystal and normal mode calculation for a neutral form of glucosamine. The spectra displayed in Fig.3 show several more intense bands having their wavenumbers written above them. From these data one can conclude that in the case of 0.1 mM solution the symmetric C-NH_3^+ bending mode observed at 1532 cm^{-1} is the dominant band in the spectrum, while there are several bands attributed to asymmetric C-NH_3^+ bending (1563, 1586 and 1652 cm^{-1}). The occurence of more than three transitions involving C-NH_3^+ group is attributed to different binding of several glucosamine molecules. Another prominent band observed in SERS spectrum of the 0.1 mM solution is found at 1165 cm^{-1}, and assigned to C-N stretching coupled with C-C stretching motion. Although the C-NH_3^+ bending bands are also distinguishable in

the SERS spectrum of 1 mM solution, a strong band at 1075 cm^{-1}, accompanied by nearby bands at 999 cm^{-1} and 1167 cm^{-1} is found. The band at 1075 cm^{-1} is attributed to C-O stretching coupled with ring C-C stretching mode of the glucose ring, while the 999 cm^{-1} band is assigned to C-O_{ring} stretching coupled with C-NH_3^+ wagging motion. All of these assignments are in agreement with previous vibrational studies on glucosamine [36], and N-acetyl-D-glucosamine [37].

What remains to be explained is the origin of different binding of glucosamine molecules.

Previous SERS studies involving glucosamine were done on metal-acetate – glucosamine complexes with or without glycine [38], or on metal-acetate-glucosamine-beta-naphtaldehyde complexes [39]. In these works colloid silver prepared from citrate reduction was used; zeta potential of the particles was -33.4 mV and the green excitation from Ar^+ laser of 514.5 nm served as an excitation source. The strongest band observed at 1394 cm^{-1} band was assigned to COO^- symmetric stretching vibration, but this band could originate either from citrate groups or from the glycine [40]. A strong band at 1586 cm^{-1} was also observed and assigned to a deformation mode of the NH_2 group. At 1244 and 1276 cm^{-1} two distinct bands were assigned to C-N and C-O stretching vibrations [36]. In conclusion, authors suggested that both –NH and –OH groups could present themselves as SERS active sites. In the SERS spectra presented here (see Supplementary Table S1 for the list of all observed bands) only glucosamine and water vibrations contribute to the bands observed in the 550 – 1700 cm^{-1} spectral interval. The bending band of water at 1630 cm^{-1} is very weak in comparison with bands from SERS spectrum (Fig.4).

Another SERS spectrum of glucosamine-AuNPs that was reported by Govindaraju et al. [12] consists of four bands in the 300 – 900 cm^{-1} interval, one of which occurs in their spectrum of pure gold colloid (493 cm^{-1}). Interestingly, their reported values of hydrodynamic particle size for AuNPs was 100.51±4.39 nm which decreased to 93.36±0.58 nm upon addition of glucosamine.

What has not been explicitly stated in previous SERS studies, but is found to be important, is that at different pH values, glucosamine exists in different ratio of concentrations of its two anomers: α and β. As reported in 2006. by Skelley and Mathies [41], glucosamine powder when dissolved consists mainly of α anomers which transform gradually into β form; the final ratio of molecules in the form of β to those in the form of α is 0.39 [41]. Virués et al. [34] used ^1H NMR for determination of the anomer concentrations at different pD values, and found that in $GlcN^+$ acid hydrogen is localized on nitrogen atom in α anomer, and is delocalized over two donor atoms in β anomer (at anomeric oxygen and at nitrogen).

In view of these facts, one can offer another interpretation for the cause of different wavenumber positions of the strongest bands observed in SERS spectra of 0.1 mM and 1 mM glucosamine solutions shown in Fig.3 and listed in Table 1. There exists a possibility that C-O stretching vibration observed at 1075 cm^{-1} in 1 mM glucosamine solution is originating from $GlcN^+$ anomers protonated at anomeric oxygen position. Negatively charged AuNPs attract positively charged glucosamine which disposes with two possibilities for preferred orientation. Since NH_3^+ group exists in both

glucosamine anomers, the C-NH_3^+ angle bending deformation modes will contribute to SERS spectra of both anomers (bands between 1530 and 1655 cm^{-1}), while the C-O sretching band (1075 cm^{-1}) will be enhanced for the β bound anomer.

For polycrystalline α and β glucose, there exist strong bands in Raman spectra by which one can clearly distinguish and identify each polymorph (in this case also each anomer): they are at 843 and 915 cm^{-1} in the Raman spectrum of α glucose, and at 901 cm^{-1} in the Raman spectrum of β glucose (Fig.5). It is therefore tempting to search for bands characteristic of α and β anomer of glucosamine in the 800 – 950 cm^{-1} interval of its SERS spectra (Fig.3). In the SERS spectrum of 0.1 mM solution, one observes bands at 831, 899 and 946 cm^{-1}, and in the SERS spectrum of 1 mM solution bands at 828, 934 and 999 cm^{-1}. All of these bands are overlapping with broad, medium intensity bands, present in spectra of both solutions, and it is not possible to confidently assign them as belonging either to α or β glucosamine anomer.

Conclusion

Surface-enhanced Raman spectra of water solutions of glucosamine mixed with surface-clean gold nanoparticles obtained by laser ablation in liquid were obtained for 0.1 mM and 1 mM concentrations. Comparison of spectra normalized to the silicon band 520.7 cm^{-1} reveal intensity enhancements of bands assigned to deformation of C-NH_3^+ angles bending motion and C-O and C-C stretching mode, supporting the hypothesis that at least two ways of binding of glucosamine to gold nanoparticles exist. Experiments by dynamic light scattering and zeta potential measurements, together with UV-VIS experiments confirm that binding of glucosamine to AuNPs took place.

Acknowledgement

This work was supported by Centre for Advanced Materials and Sensing Devices, project number EK-EFRR-KK.01.1.1.01.0001. Zetasizer Ultra (Malvern Panalytical) was purchased by the project UIP-2017-05-7337 financially supported by the Croatian Science Foundation.

Table 1. Observed bands in SERS spectra of 0.1 mM and 1 mM solutions of glucosamine hydrochloride mixed in 1.1 v/v with AuNP colloid (cm^{-1}).

0.1 mM $GlcN^+$ solution+AuNP	1 mM $GlcN^+$ solution+AuNP	assignment
1652	1642	C-NH_3^+ bending, asym.
1586	1582	C-NH_3^+ bending, asym.
1563		C-NH_3^+ bending, asym.
1532	1537	C-NH_3^+ bending, sym.
1457		COH bending
1438	1441	COH bend.+CH_2 scissoring
1375	1375	CH wagging
	1353	CH, OH bending
1334		CH bending
1312	1320	CH_2 twisting
1270	1260	CH wagging
1236		CH_2 twisting
1221		CH twist + COH bending
1165	1167	CN stretching+CC stretching
1142		CC stretching
	1075	CO stretching + CC stretching
1049		COring stretching
1026	1026	ring stretching + CN stretching
992	999	COring stretching+CNH_3^+ bend
946	934	CH rocking
899		CH rocking
831	828	CH_2 rocking
	733	OH torsion
	643	ring bending
596		OH torsion

References

1. http://www.nccih.nih.gov/health/glucosamine-and-chondroitin-for-osteoarthritis
2. M. G. Papich in Saunders Handbook of Veterinary Drugs (Fourth Edition), 2016. https://www.elsevier.com/books/saunders-handbook-of-veterinary-drugs/9780323244855
3. H.-D. Klenk, C,. Schotischek, R. Rott, The Molecular Biology of Influenza Virus Pathogenicity, Virology 49 (1972) 723-734. https://www.ncbi.nlm.nih.gov/pmc/articles/PMC7173235/
4. J. Sebag, Macromolecular structure of the corpus vitreus, Prog. Polymer. Sci. 23 (1998) 415-446. https://www.sciencedirect.com/science/article/pii/S007967009700035X
5. S. Stridh, F. Palm, P. Hansell, Renal interstitial hyaluronan: functional aspects during normal and pathological conditions, Am. J. Physiol. Regul. Integr. Comp. Physiol. 302 (2012) R1235. https://journals.physiology.org/toc/ajpregu/302/11
6. K. T. Dicker, L. A. Gurski, S. Pradhan-Bhatt, R. L. Witt, M. C. Farach-Carson, X. Jia, Hyaluronan: a simple polysaccharide with diverse biological functions Acta Biomaterialia 10 (2014) 1558-1570. https://pubmed.ncbi.nlm.nih.gov/24361428/
7. J. Qu, X. Zhao, Y. Liang, Y. Xu, P. X. Ma, B. Guo, Degradable conductive injectable hydrogels as novel antibacterial, anti-oxidant wound dressings for wound healing, Chem. Eng. J. 362 (2019) 548 – 560. https://www.sciencedirect.com/science/article/abs/pii/S1385894719300348
8. R. Song, M. Murphy, C. Li, K. Ting, C. Soo, Z. Zheng, Current development of biodegradable polymeric materials for biomedical applications, Drug Design, Development and Therapy 12 (2018) 3117 – 3145. https://pubmed.ncbi.nlm.nih.gov/30288019/
9. G. D. Mogosanu, A. M. Grumezescu, Natural and synthetic polymers for wounds and burns dressing, Int. J. Pharmaceutics 463 (2014) 127 – 136. https://pubmed.ncbi.nlm.nih.gov/24368109/
10. H. Liu, C. Wang, C. Li, Y. Qin, Z. Wang, F. Yang, Z. Li, J. Wang, A functional chitosan-based hydrogel as a wound dressing and drug delivery system in the treatment of wound healing, RSC Advances 8 (2018) 7533. https://pubs.rsc.org/en/content/articlelanding/2018/ra/c7ra13510f#!divAbstract
11. O. Stamatoiu et al.: Nanoparticles in Liquid Crystals and Liquid Crystalline Nanoparticles, In: Tschierske, C. (eds) Liquid Crystals. Topics in Current Chemistry, vol 318, Springer Berlin, Heidelberg. https://doi.org/10.1007/128_2011_233
12. S. Govindaraju, M. Ramasamy, R. Baskaran, S. J. Ahn, K. Yun, Ultraviolet light and laser irradiation enhances the antibacterial activity of glucosamine-functionalized gold nanoparticles, Int. J. of Nanomedicine 10 (2015) 67 – 78. https://www.dovepress.com/ultraviolet-light-and-laser-irradiation-enhances-the-antibacterial-act-peer-reviewed-article-IJN

13. A. Silvestri, V. Zambelli, A. M. Ferretti, D. Salerno, G. Bellani, L. Polito, Design of functionalized gold nanoparticle probes for computed tomography imaging, Contrast Media & Molecular Imaging 11 (2016) 405 – 414. https://pubmed.ncbi.nlm.nih.gov/27377033/
14. S. Shikha, K. G. Thakur, M. S. Bhattacharya, Facile fabrication of lipase to amine functionalized gold nanoparticles to enhance stability and activity, RSC Advances 7 (2017) 42845, https://pubs.rsc.org/en/Content/ArticleLanding/RA/2017/C7RA06075K#!divAbstract
15. Y. Liu, I. M. Hsing, Cancer Specific targeting by Glucosamine Coated Gold Nanoparticles In Vitro and In Vivo, J. Biomaterials and Tissue Engineering 5 (2015) 687 – 696. https://www.ingentaconnect.com/content/asp/jbte/2015/00000005/00000009/art00003;jsessionid=n6902boug3qf.x-ic-live-03
16. C. Bravin, V. Amendola: Wide range detection of C-Reactive protein with a homogeneous immunofluorimetric assay based on cooperative fluorescence quenching assisted by gold nanoparticles, Biosensors and Bioelectronics, 169 (2020) 112591. https://www.sciencedirect.com/science/article/abs/pii/S0956566320305819
17. S. Crivellaro, A. Guadagnini, D. Muñetón Arboleda, D. Schinca, V. Amendola: A system for the synthesis of nanoparticles by laser ablation in liquid that is remotely controlled with PC or smartphone, Rev. Sci. Instrum. 90 (2019) 033902. https://aip.scitation.org/doi/full/10.1063/1.5083811
18. V. Merk, C. Rehbock, F. Becker, U. Hagemann, H. Nienhaus, S. Barcikowski: In situ non-DLVO stabilization of surfactant-free, plasmonic gold nanoparticles: effect of Hofmeister's anions, Langmuir 30 (2014) 4213–4222. https://pubs.acs.org/doi/abs/10.1021/la404556a
19. C. Virués, J. Hernández, I. Higuera-Ciapara, E. Martínez-Benavidez, J. L. Olivares-Romero, R. E. Navarro, M. Inoue, Formulation of anomerization and protonation in d-glucosamine, based on ^{1}H NMR, Carbohyd. Res. 490 (2020) 107952. https://www.sciencedirect.com/science/article/abs/pii/S0008621519306494
20. https://imagej.net/Welcome
21. Gaussian 09, Revision A.02, M. J. Frisch, G. W. Trucks, H. B. Schlegel, G. E. Scuseria, M. A. Robb, J. R. Cheeseman, G. Scalmani, V. Barone, G. A. Petersson, H. Nakatsuji, X. Li, M. Caricato, A. Marenich, J. Bloino, B. G. Janesko, R. Gomperts, B. Mennucci, H. P. Hratchian, J. V. Ortiz, A. F. Izmaylov, J. L. Sonnenberg, D. Williams-Young, F. Ding, F. Lipparini, F. Egidi, J. Goings, B. Peng, A. Petrone, T. Henderson, D. Ranasinghe, V. G. Zakrzewski, J. Gao, N. Rega, G. Zheng, W. Liang, M. Hada, M. Ehara, K. Toyota, R. Fukuda, J. Hasegawa, M. Ishida, T. Nakajima, Y. Honda, O. Kitao, H. Nakai, T. Vreven, K. Throssell, J. A. Montgomery, Jr., J. E. Peralta, F. Ogliaro, M. Bearpark, J. J. Heyd, E. Brothers, K. N. Kudin, V. N. Staroverov, T. Keith, R. Kobayashi, J. Normand, K. Raghavachari, A. Rendell, J. C. Burant, S. S. Iyengar, J. Tomasi, M. Cossi, J. M. Millam, M. Klene, C. Adamo, R. Cammi, J. W. Ochterski, R. L. Martin, K. Morokuma, O. Farkas, J. B. Foresman, and D. J. Fox, Gaussian, Inc., Wallingford CT, 2016.

22. W. T. A. Harrison, H. S. Yathirajan, B. Narayana, T. V. Sreevidya and B. K. Sarojini, Redetermination of [alpha]-D-glucosamine hydro-chloride: elucidation of the hydrogen-bonding scheme, Acta Cryst. (2007). E63, o3248; https://doi.org/10.1107/S1600536807024506
23. R. Dovesi, R. Orlando, B. Civalleri, C. Roetti, V. R. Saunders, and C. M. Zicovich-Wilson, CRYSTAL: a computational tool for the ab initio study of the electronic properties of crystals, Z. Kristallogr. 220, (2005) 571. https://www.degruyter.com/document/doi/10.1524/zkri.220.5.571.65065/html
24. R. Dovesi, V. R. Saunders, C. Roetti, R. Orlando, C. M. Zicovich-Wilson, F. Pascale, B. Civalleri, K. Doll, N. M. Harrison, I. J. Bush, P. D'Arco, and M. Llunell, CRYSTAL09 User's Manual (University of Torino, Torino, 2009). https://www.crystal.unito.it/manuals/crystal09.pdf
25. John P. Perdew, K. Burke, and M. Ernzerhof, Phys. Phys Rev. Lett. 77, 3865. Erratum Phys. Rev. Lett. 78, 1396 (1997) https://journals.aps.org/prl/abstract/10.1103/PhysRevLett.77.3865
26. John P. Perdew, Adrienn Ruzsinszky, Gábor I. Csonka, Oleg A. Vydrov, Gustavo E. Scuseria, Lucian A. Constantin, Xiaolan Zhou, and Kieron Burke, Phys. Rev. Lett. 100, 136406; Erratum Phys. Rev. Lett. 102, 039902 (2009) https://journals.aps.org/prl/abstract/10.1103/PhysRevLett.100.136406
27. C. Gatti, V.R. Saunders, C. Roetti,"Crystal-field effects on the topological properties of the electron-density in molecular-crystals - the case of urea",J. Chem. Phys. 101, (1994) 10686-10696. https://aip.scitation.org/doi/10.1063/1.467882
28. E. Apra, M. Causa, M. Prencipe, R. Dovesi and V.R. Saunders, On the structural properties of NaCl. An ab initio study of the B1-B2 phase transition, J. Phys. Condens. Matter 5, (1993) 2969-2976 https://iopscience.iop.org/article/10.1088/0953-8984/5/18/019/meta
29. http://crysplot.crystalsolutions.eu/web_pages_yves3/vibration.html
30. G. M. Brown, H. A. Levy, Alpha-D-glucose: Further refinement based on neutron-diffraction data, Acta Cryst. B35 (1979) 656. https://onlinelibrary.wiley.com/doi/epdf/10.1107/S0567740879004374?sentby=iucr
31. W. G. Ferrier, The crystal and molecular structure of beta-D-glucose, Acta Cryst. 16 (1963) 1023. https://onlinelibrary.wiley.com/doi/abs/10.1107/S0365110X63002693
32. V. Amendola, L. Litti, M. Meneghetti: LDI-MS assisted by chemical-free gold nanoparticles: enhanced sensitivity and reduced background in the low-mass region, Anal. Chem. 85 (2013) 11747 – 11754. https://pubs.acs.org/doi/abs/10.1021/ac401662r
33. V. Amendola, R. Pilot, M. Frasconi, O. M. Maragò, M. A. Iatì: Surface plasmon resonance in gold nanoparticles: a review, J. Phys.: Condens. Matter 29 (2017) 203002. https://iopscience.iop.org/article/10.1088/1361-648X/aa60f3/meta
34. C. Virués, J. Hernández, I. Higuera-Ciapara, E. Martínez-Benavidez, J. L. Olivares-Romaro, R. E. Navarro, M. Inoue, Formulation of anomerization and protonation in d-glucosamine, based on 1H NMR, Carbohydr. Res. 490 (2020)

107952, https://www.sciencedirect.com/journal/carbohydrate-research/vol/490/suppl/C
35. M. Moskovits, Surface-enhanced spectroscopy, Rev. Mod. Phys. 57 (1985) 783. https://journals.aps.org/rmp/abstract/10.1103/RevModPhys.57.783
36. C. Y. She, N. D. Dinh, A. T. Tu: Laser Raman scattering of glucosamine, N-acetylglucosamine and glucuronic acid, Biochim. Biophys. Acta 372 (1974) 345. https://www.sciencedirect.com/science/article/abs/pii/0304416574901962
37. I. Kouach-Alix, G. Vergoten: A vibrational molecular force field of model compounds with biological interest. V. Harmonic dynamic of N-acetyl-alpha-D-glucosamine in the crystalline state, J. Mol. Struct. 323 (1994) 39. https://www.sciencedirect.com/science/article/abs/pii/0022286093079694
38. Y.Ye, J. Hu, Y. Zeng, SERS study of some novel metal complexes derived from D-glucosamine, J. Raman Spectrosc. 32 (2001) 1018. https://analyticalsciencejournals.onlinelibrary.wiley.com/doi/abs/10.1002/jrs.795
39. J. Shen, Y. Ye, J. Hu, H. Shen, Z. Le, Surface-enhanced Raman spectra study of metal complexes of N-D-glucosamine beta-naphtaldehyde and glycine and their interaction with DNA, Spectrochim. Acta A 57 (2001) 551-559. https://www.sciencedirect.com/science/article/pii/S1386142500004029?via%3Dihub
40. M. Kerker, O. Siiman, L. A. Bumm, D.-S. Wang, Surface enhanced raman scattering (SERS) of citrate ion adsorbed on colloidal silver, Applied Optics 19 (1980) 3253. https://www.osapublishing.org/ao/abstract.cfm?uri=ao-19-19-3253
41. A. M. Skelley, R. A. Mathies: Rapid on-column analysis of glucosamine and its mutarotation by microchip capillary electrophoresis, J. Chromatogr. A 1132 (2006) 304 – 309. https://www.sciencedirect.com/science/article/abs/pii/S0021967306014804?via%3Dihub

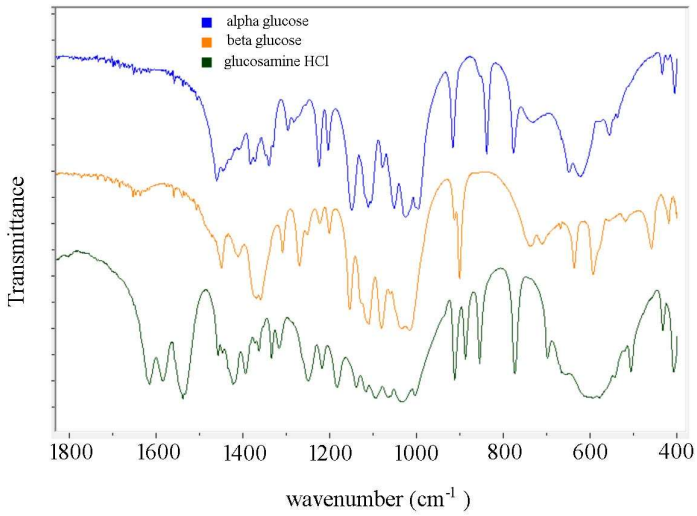

Supplementary Fig.S1: Infrared spectra of polycrystalline α-glucose, β-glucose and glucosamine·HCl in the interval 400-1800 cm^{-1}.

Supplementary Table S1. Comparison of observed bands in Raman spectra of 1M glucosamine water solution ($GlcN^+$) and polycrystalline glucosamine HCl with calculated valuesof normal modes of neutral glucosamine $GlcN^o$ and phonons in the crystal. Atomic motions in phonon modes can be viewed online [29] once the CRYSTAL09 output is uploaded. The output is part of Supplementary Information.

observed Raman solution 1M	observed Raman crystal 295 K	calculated phonons for polycrystalline $GlcN^+HCl$ (CRYSTAL09)	calculated normal modes of $GlcN^o$ (Gaussian09)	normal mode of $GlcN^o$ description
3399 vbr	3350 sh	3331, 3321, 3307, 3302	3853,3827	OH stretching
	3320	3210, 3209, 3154, 3148	3821,3804	OH stretching
3257 vbr	3290	3407,3408	3600	asym. stretching NH2
		3374,3377	3509	sym. stretching NH2
	3096	3079,3079, 3007,3008	3090,3077,3071,	CH stretching
	3042	2985,2985,2994,2995	3056,3041	CH stretching
2972	2972	2966,2967	3018	sym. CH2 stretching
	2969	2959,2960	3007	CH stretching
2951 sh	2945			
	2933	2923,2923		
2908	2913			
2875 sh	2884			
	2843			
		2517,2521* N-H ···O		
1639 br				bending H2O
	1616	1614, 1612	1656	bending NH2
1552	1585			
1525	1541	1551,1548,1537, 1536		
1475				
1461	1460	1440	1509	bending CH2
	1451	1423,1425,1438	1450	bending CH
1419	1432	1411,1411,1415,1417	1444	CH i OH bending
1389			1431	CH i OH bending
	1396		1417	CH2 bending
	1385	1387,1388	1411,1409	CH rocking
	1375	1368	1375	CH wagging
1356	1366	1361,1367	1367	CH twisting
1332	1353	1350,1353,1358	1358	CH and OH wagging
	1334	1331,1334,1342	1345	CH bending
1276	1318	1317,1319,1327	1291	CH2 twisting
1261		1279,1283,1296,1298	1286	COH bending
	1265		1277	COH bending
1236			1252	COH bending
		1238,1248, 1248	1203	COH bending
1189	1239	1211,1214,1231	1199	NH2 twisting
1137	1220	1164,1170,1182,1186	1181	COH+CH bending
1110	1186	1136,1137,1145,1146	1163	CCC bending
	1137 s	1123,1125,1127	1141	CC stretching
		1103, 1116	1120	OC and CC stretching
1077	1109	1074,1086,1099	1112	N-Cand CC stretching
1048	1091	1055,1057,1065	1083	C-O stretching
	1060	1042,1044,1045	1077	CC and CN stretching
	1041		1069	CH2 rocking
			1049	CO and CC stretching
982	1004	1023, 1024	1026	NH2 twist+COH bend
964		1000, 1004	1003	CC stretching
	937 vw		944	ring stretching
899	914	915, 919		
862	889 ms	874	887	NH2, CH2 wagging
	857 ms	869		

Supplementary Table S1, continued

observed Raman solution 1M	observed Raman crystal 295 K	calculated phonons for polycrystalline $GlcN^+HCl$ (CRYSTAL09)	calculated normal modes of $GlcN^o$ (Gaussian09)	normal mode of $GlcN^o$ description
847		849, 850	877	NH2 wagging
		795, 803	846	CO stretching
740 vw	771	769, 770	765	OCO bending
	698	695, 699	684	CCC bending
		643, 647		
	609	604, 608, 609, 613		
582	579	575, 580	576	OCO i CCO bending
543	544	536, 539	553	ring bending
514	520	522, 522	516	ring bending
496 sh	508 s	500, 502	505	OCC bending
444			438	torsion OH
425	431	427	428	torsion OH
	411 sh	409, 423	403	ring bending
404	405	407, 409	378	torsion OH
	372	360, 364	348	NH2 rocking,OH torsion
338	336	326, 353, 357	341	OH
			326	NH2 rocking,OH torz.
	288	285, 295, 310	284	torsion C15C22
	277 vw sh	270, 280	271	torsion C13C21
	249, 237	251, 255,261,265	256	torsion OH
			245	bending OCC
	212	214, 216, 221, 224	227	torsion OH
			216	torsion C15C22
	190	198, 201		
	166	152, 157, 162, 168	149	torsion C13C21
	128 sh	137		
	118	120, 122, 124		
	108	102, 107	111	skeletal deformation
	93	88	87	skeletal deformation
	75	82		
	68	68		
	56	51, 62,63	56	torsion CH2OH
		44		